

CrossMark
click for updatesCite this: *Chem. Sci.*, 2017, 8, 2569

Electrochemical promotion of catalysis over Pd nanoparticles for CO₂ reduction†

Fan Cai,^{ac} Dunfeng Gao,^a Hu Zhou,^b Guoxiong Wang,^{*a} Ting He,^{ac} Huimin Gong,^a Shu Miao,^a Fan Yang,^a Jianguo Wang^b and Xinhe Bao^{*a}

Electrochemical promotion of catalysis (EPOC) has been shown to accelerate the rate of many heterogeneous catalytic reactions; however, it has rarely been reported in low-temperature aqueous electrochemical reactions. Herein, we report a significant EPOC effect for the CO₂ reduction to generate formate over Pd nanoparticles (NPs) in a 1 M KHCO₃ aqueous solution. By applying a negative potential over differently-sized Pd NPs, the rate of formate production is greatly improved as compared to that at an open-circuit voltage, with a rate enhancement ratio ranging from 10 to 143. The thermocatalytic and electrocatalytic reduction of CO₂ compete with each other and are promoted by the applied negative potential and H₂ in the feeds, respectively. Inspired by the EPOC effect, a composite electrode containing Pd/C and Pt/C catalysts on different sides of a carbon paper was constructed for catalyzing the CO₂ reduction without adding H₂ to the feeds. Water electrolysis over Pt NPs generates H₂, which then effectively promotes formate production over Pd NPs.

Received 10th November 2016
Accepted 24th December 2016

DOI: 10.1039/c6sc04966d

www.rsc.org/chemicalscience

Introduction

Electrochemical promotion of catalysis (EPOC), discovered by M. Stoukides and C. Vayenas in the 1980s,^{1,2} has been widely investigated in more than 100 heterogeneous catalytic reactions^{3–6} on either metal or metal oxide surfaces, which are interfaced with a solid⁷ or an aqueous electrolyte solution.^{8–14} By applying an electrical current between the working electrode, coated with catalyst, and the counter electrode, the electronic properties of the supported catalyst can be tuned, accompanied by the alteration in the adsorption strength of the reactants, and in some cases, a significant enhancement in the catalytic performance can be observed. To date, only a few reports have demonstrated the EPOC effect in an aqueous electrolyte solution at ambient temperature for reactions such as the H₂ oxidation,^{8,9} hydrocarbon isomerization,^{10,11} CO oxidation,^{12,13} and hydrazine oxidation.¹⁴ Herein, we report that the EPOC effect can also be observed for electrochemical reduction reactions such as the reduction of CO₂ in an aqueous electrolyte solution at ambient temperature.

The reduction of carbon dioxide to produce formic acid is an attractive route to store renewable electricity and an important

strategy for the utilization of carbon cycle.^{7,15–19} However, CO₂ is thermodynamically stable and notoriously unreactive; therefore, high reaction temperatures^{7,20–23} and high overpotentials^{24–27} are usually essential to activate and transform CO₂ during thermocatalysis and electrocatalysis. Herein, we report a significant EPOC effect for the CO₂ reduction to produce formate over Pd nanoparticles (NPs) in a 1 M KHCO₃ aqueous solution at ambient temperature. Thermocatalytic and electrocatalytic reduction of CO₂ over Pd nanoparticles (NPs) occur simultaneously and compete with each other, which are promoted by the applied negative potential and H₂ in the feeds, respectively. The shared reaction intermediate, namely HCOO*, is formed over the Pd NPs and is proposed as the origin of the EPOC effect during the thermocatalytic and electrocatalytic reduction of CO₂. Inspired by the EPOC effect, a Pd/C–Pt/C composite electrode was constructed for the CO₂ reduction, such that the addition of H₂ to the feeds could be avoided. H₂ generated from the electrolysis of water over Pt NPs effectively promotes formate production over Pd NPs.

Results and discussion

Carbon-supported Pd NPs were prepared using sodium citrate as a stabilizing agent and NaBH₄ as a reducing agent.²⁸ Each sample was named on the basis of the average size of Pd NPs present in it, such as 3.7 nm Pd indicates that Pd NPs in the Pd/C catalyst have an average particle size of 3.7 nm (Fig. S1†). The catalyst ink, containing Pd/C and Nafion ionomer, was deposited on a piece of carbon paper (Toray TGP-H-060) with a microporous layer and dried to serve as a porous electrode for

^aState Key Laboratory of Catalysis, CAS Center for Excellence in Nanoscience, Dalian Institute of Chemical Physics, Chinese Academy of Sciences, 116023, Dalian, China. E-mail: wanggx@dicp.ac.cn; xhbao@dicp.ac.cn

^bCollege of Chemical Engineering, Zhejiang University of Technology, 310032, Hangzhou, China

^cUniversity of Chinese Academy of Sciences, 100039, Beijing, China

† Electronic supplementary information (ESI) available. See DOI: 10.1039/c6sc04966d



CO₂ reduction in a 20% H₂/CO₂-saturated 1 M KHCO₃ solution. To quantify the EPOC effect, the rate enhancement ratio was defined as follows:³

$$\rho = r/r_0 \quad (1)$$

where r and r_0 are the rates of the promoted (by applying negative potentials) and unpromoted (at open-circuit voltage, OCV) reactions, respectively. In this study, all r values measured under different atmospheres or over different electrodes are calculated by the following equation:

$$r = \frac{\text{total amount of formate generated in one hour (in mol)}}{\text{total amount of Pd in electrode (in milligram)} \times 1 \text{ h}} \quad (2)$$

CO₂ reduction experiments were conducted in an H-cell, as shown in Fig. 1a. The porous electrode coated with Pd/C catalyst was immersed in a 1 M KHCO₃ aqueous solution, and 20% H₂/CO₂ was fed into the cathode chamber for the CO₂ reduction reaction at OCV and different negative potentials. The maximum temperature increment of the electrolyte solution was 0.8 °C during the constant-potential electrolysis for 1 h, and the effect of temperature on the formate production rate at OCV and different negative potentials can be ignored. Fig. 1b shows the rate enhancement ratio for the formate production at different negative potentials compared to that at OCV over differently-sized Pd NPs. There are volcano-like curves for the value of ρ over differently-sized Pd NPs within the studied potential range. The value of ρ is 54 over 2.4 nm Pd at -0.1 V and reaches the maximum value of 143 at -0.2 V. Further negatively shifting the potential to -0.3 V and -0.4 V would decrease the rate enhancement ratio to 95 and 39, respectively. The ratio over 3.7 nm Pd increases from 58 to 119 when the potential is shifted from -0.1 V to -0.2 V and drops to 100 and 17 at -0.3 V and -0.4 V, respectively. The ratio over 7.8 nm Pd is obviously smaller than that over 2.4 nm Pd and 3.7 nm Pd, and the maximum ratio over 7.8 nm Pd is 23 at -0.2 V. The reaction of adsorbed hydrogen on Pd hydride surface with CO₂ to form adsorbed HCOO* is considered as the rate-determining step for CO₂ reduction.¹⁶ Upon negatively shifting the potential from -0.1 V to -0.4 V, the hydrogen adsorption strength on the Pd

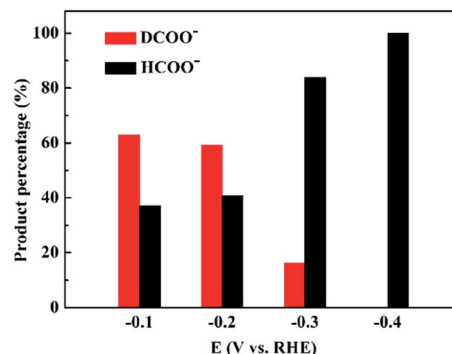


Fig. 2 HCOO⁻ and DCOO⁻ percentages for the CO₂ reduction over 3.7 nm Pd at different negative potentials in 20% D₂/CO₂-saturated 1 M KHCO₃ solution.

hydride surface is weakened due to a favored hydrogen evolution reaction. Therefore, the optimum adsorption strength for surface-adsorbed hydrogen to react with CO₂ occurs at -0.2 V, resulting in the highest ρ value. Since small-sized Pd NPs prefer to adsorb more hydrogen over coordinatively unsaturated sites,²⁹ the ρ value is much higher over 2.4 nm Pd as compared to that over 3.7 nm Pd and 7.8 nm Pd at -0.4 V.

To investigate the origin of the EPOC effect during CO₂ reduction, an isotope-labeling experiment was conducted by replacing 20% H₂/CO₂ with 20% D₂/CO₂, and the products were analyzed by nuclear magnetic resonance (NMR) spectroscopy. PdD_x could also be generated under D₂ atmosphere, and the properties of PdD_x were close to those of PdH_x; thus, it was suggested that the electrochemical measurements under 20% D₂/CO₂ atmosphere were comparable to those under 20% H₂/CO₂ atmosphere.^{30–32} HCOO⁻ and DCOO⁻ were quantified by ¹H-NMR and ²H-NMR spectra, respectively. The amount of D₂O and HDO in the electrolyte solution after constant-potential electrolysis at -0.2 V for 1 h was also quantified by ²H-NMR spectra, which is 0.028%, whereas the natural abundance of D is about 0.015%.³³ Therefore, non-electrochemical exchange between adsorbed D and H⁺ could be ignored,³⁴ and DCOO⁻ and HCOO⁻ were considered to be produced from the CO₂ + D₂ thermocatalytic reaction and CO₂ electrocatalytic reaction, respectively. Fig. 2 shows the percentage of HCOO⁻ and DCOO⁻ formed over 3.7 nm Pd at different negative potentials. The percentage of DCOO⁻ is higher than that of HCOO⁻ at -0.1 V and -0.2 V, which sharply decreases at -0.3 V and reaches below the detection limit at -0.4 V. Thus, the thermocatalytic and electrocatalytic reduction of CO₂ occur simultaneously and compete with each other when applying negative potentials over Pd NPs.

We also measured the electrocatalytic reduction of CO₂ without adding H₂ to the feeds. As shown in Fig. 3, S2 and S3,[†] the current density becomes unstable at negatively shifted potentials, which is caused by poisoning from trace CO, a minor side product from the CO₂ electroreduction.^{16,35–37} With the addition of H₂, the stability of current density increases, indicating that the electrocatalytic reduction of CO₂ is stabilized. X-ray diffraction (XRD) patterns, of 3.7 nm Pd under different atmospheres were obtained to investigate the active phase of Pd

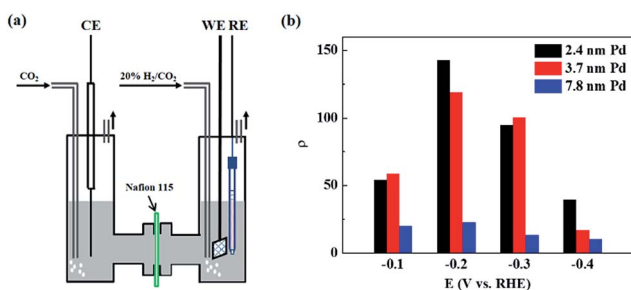


Fig. 1 (a) Schematic of the H-cell for CO₂ reduction. (b) Rate enhancement ratios for formate production at different negative potentials compared to those at OCV over differently-sized Pd NPs in 20% H₂/CO₂-saturated 1 M KHCO₃ solution.



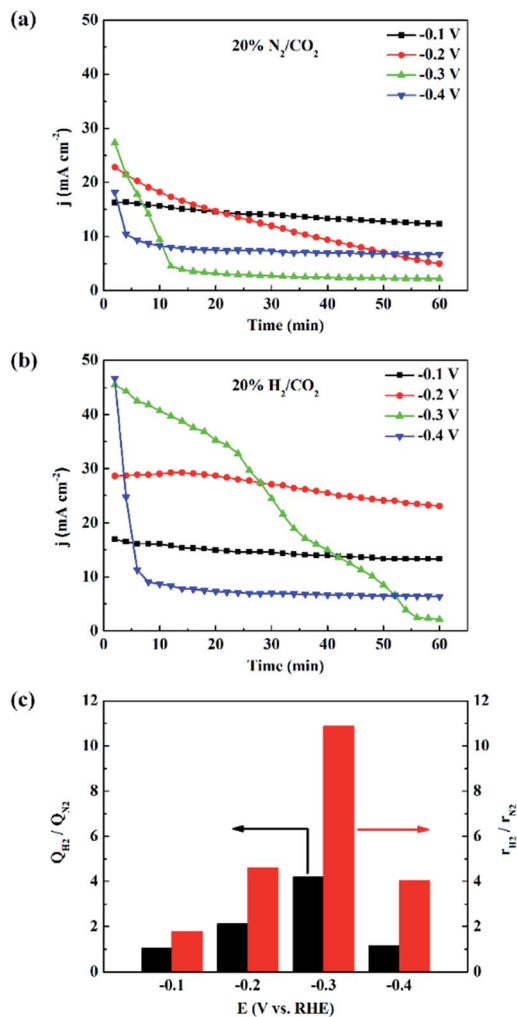


Fig. 3 Chronoamperometry curves of 3.7 nm Pd in 20% N₂/CO₂-saturated (a) and 20% H₂/CO₂-saturated (b) 1 M KHCO₃ solution. (c) Enhancement of electric charge ($Q_{\text{H}_2}/Q_{\text{N}_2}$) ratio and formate production rate ratio ($r_{\text{H}_2}/r_{\text{N}_2}$) over 3.7 nm Pd at different negative potentials in 20% N₂/CO₂ and 20% H₂/CO₂-saturated 1 M KHCO₃ solutions.

NPs, as shown in Fig. S4.† XRD pattern of 3.7 nm Pd under 20% N₂/CO₂ atmosphere matches well with that of Pd (JCPDS 46-1043), and the diffraction peak of the Pd (111) plane is located at 39.9°. When the atmosphere is switched to 20% H₂/CO₂, the diffraction peak of the Pd (111) plane quickly shifts to 38.8°, accompanied by a shift in all the other peaks. The pattern is consistent with that of PdH_{0.706} (JCPDS 18-0951), which is facily generated under H₂ atmosphere. Since the state and structure of the supported Pd NPs are not affected by water,³⁸ the PdH_x active phase is expected to be stable in 20% H₂/CO₂-saturated 1 M KHCO₃ solution.

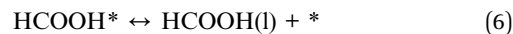
Fig. 3c shows the electric charge ratios over 3.7 nm Pd at various potentials, calculated from the $I-t$ plots, in Fig. 3a and b. At -0.1 V, the electric charge does not change over Pd NPs because surface PdH_x is stable and the rate of proton reduction can meet the requirement for the CO₂ electroreduction. At -0.2 V, CO₂ electroreduction is accelerated, and the rate of

proton reduction cannot match the rate of CO₂ electroreduction, resulting in a decrease of current density. The enhancement of the electric charge ratio is the highest at -0.3 V since the addition of H₂ effectively stabilizes surface PdH_x that tends to decompose through hydrogen evolution. This enhancement of electric charge ratio indicates that the electrocatalysis is to some extent also promoted by H₂ in the feeds, which has not been reported earlier.

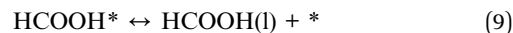
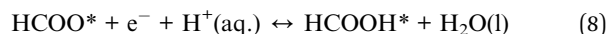
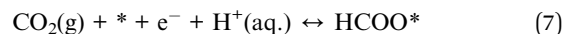
The rate of formate production was enhanced when the reaction atmosphere was changed from 20% N₂/CO₂ to 20% H₂/CO₂. Fig. 3c shows the enhancement ratio of $r_{\text{H}_2}/r_{\text{N}_2}$ over 3.7 nm Pd at different negative potentials, where r_{H_2} and r_{N_2} represent the formate production rates in 20% H₂/CO₂ and 20% N₂/CO₂-saturated electrolyte solutions, respectively. The enhancement ratio of formate production rates is higher than that of electric charge accumulated in 1 h. For instance, r_{H_2} at -0.2 V reaches about 1.9 mol_{formate} mg_{Pd}⁻¹ h⁻¹, and $r_{\text{H}_2}/r_{\text{N}_2}$ is more than twice that of $Q_{\text{H}_2}/Q_{\text{N}_2}$. The additional improvement is considered as a contribution from the thermocatalytic reaction,³⁹ also identified in the isotope labeling experiment. The significant potential dependence of the $r_{\text{H}_2}/r_{\text{N}_2}$ and $Q_{\text{H}_2}/Q_{\text{N}_2}$ values over 3.7 nm Pd is attributed to the instability of Pd hydride and CO poisoning at more negative potentials during the electrocatalytic reduction of CO₂. Similar enhancement effects over 2.4 nm and 7.8 nm Pd are shown in Fig. S2 and S3.† Since the strong hydrogen adsorption on small-sized Pd NPs could stabilize the surface Pd hydride, the current densities over 2.4 nm Pd were more stable than those over 3.7 nm Pd (Fig. 3 and S2.†). Therefore, the $r_{\text{H}_2}/r_{\text{N}_2}$ and $Q_{\text{H}_2}/Q_{\text{N}_2}$ values over 2.4 nm Pd are smaller than those over 3.7 nm Pd. The lack of potential dependence of $r_{\text{H}_2}/r_{\text{N}_2}$ and $Q_{\text{H}_2}/Q_{\text{N}_2}$ over 7.8 nm Pd indicates that surface Pd hydride is difficult to form over large-sized Pd NPs, as also confirmed by the unstable current densities shown in Fig. S3.†

Based on the abovementioned results, thermocatalytic and electrocatalytic reduction of CO₂ occur simultaneously as follows:^{40–42}

(a) Thermocatalytic reduction reaction



(b) Electrocatalytic reduction reaction



where * and H represent the palladium hydride active phase and the free H atom adsorbed on the catalyst surface, respectively. HCOO* and HCOOH* represent the corresponding



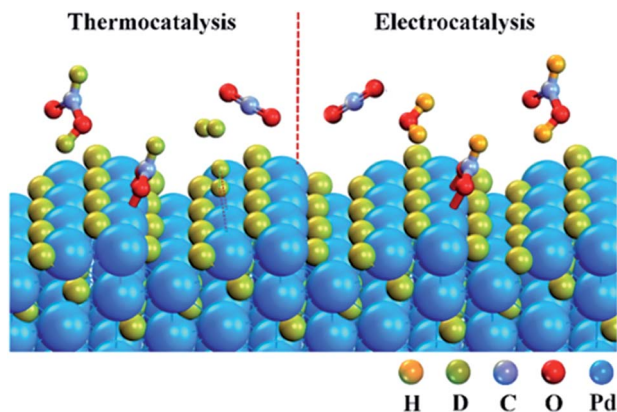


Fig. 4 Schematic of heterogeneous thermocatalytic (left) and electrocatalytic (right) reduction of CO_2 over Pd NPs conducted in a $\text{CO}_2 + \text{D}_2$ atmosphere.

intermediate species. It is clear from eqn (4) and (7) that the thermocatalytic and electrocatalytic reduction of CO_2 share the same intermediate species HCOO^* . Recent research on hydrazine electrooxidation indicates that the mechanistic origin of the EPOC effect lies in structurally similar activated transition states and/or adsorbed surface intermediates arising from hydrazine oxidation and decomposition.¹⁴ Therefore, the negative electrode potentials could affect and promote the heterogeneous catalytic reduction of CO_2 .

Fig. 4 shows the schematic of $\text{CO}_2 + \text{D}_2$ reduction over Pd NPs. D_2 is split into D atoms on the surface of Pd NPs, which subsequently diffuse into the Pd lattice to form the PdD_x phase. The atomic D on the PdD_x surface, derived from D_2 dissociation, reacts with CO_2 to form DCOO^- via the thermocatalytic pathway, whereas H^+ in water reacts with CO_2 to form HCOO^- via the electrocatalytic pathway. At -0.1 V and -0.2 V, the electrocatalytic reduction rate is constrained due to the low overpotentials and the percentage of HCOO^- is lower than that of DCOO^- . Upon increasing the overpotential, the electrocatalytic reduction rate is accelerated, exceeding the thermocatalytic rate, and thus the electrocatalytic reduction pathway dominates for CO_2 reduction at -0.4 V (Fig. 2).

H_2 generated from the electrolysis of water is promising for practical applications in CO_2 reduction. Within the potential range for the CO_2 reduction via $\text{CO}_2 + \text{H}_2$ reaction, the hydrogen evolution reaction can occur over Pt NPs, which would provide H_2 by the electrolysis of water at the same negative potentials.^{43,44} We designed a composite electrode in which 3.7 nm Pd was deposited on the microporous layer, whereas commercial Pt/C catalyst was deposited on the other side of the carbon paper. The cross-sectional scanning electron microscopy (SEM) image and corresponding energy-dispersive X-ray spectroscopy mapping image of the electrode are shown in Fig. 5a and S5.† As illustrated in Fig. 5b, the Pt/C and Pd/C catalyst layers are separated by the carbon paper with a microporous layer, and H_2 generated over Pt NPs diffuses across the carbon paper or the electrolyte solution towards the Pd NPs, which promotes the thermocatalytic and electrocatalytic reduction of CO_2 over Pd NPs. The current density is clearly improved and stabilized after

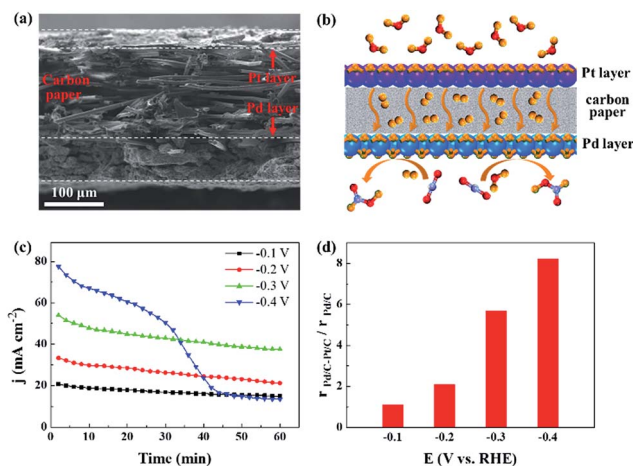


Fig. 5 CO_2 electroreduction over the Pd/C–Pt/C composite electrode in 20% N_2/CO_2 -saturated 1 M KHCO_3 solution. (a) Cross-sectional SEM image of the Pd/C–Pt/C composite electrode. (b) Schematic for the reaction mechanism in the Pd/C–Pt/C composite electrode. (c) Chronoamperometry curves of the Pd/C–Pt/C composite electrode at different negative potentials. (d) Rate enhancement ratio for formate production over the Pd/C–Pt/C composite electrode versus the Pd/C electrode at different negative potentials.

depositing Pt/C catalyst on the opposite side of the Pd/C catalyst layer (Fig. 3a and 5c). The activity and selectivity of the Pt/C electrode, used as a control in this study, were also measured, and only H_2 was produced (Fig. S6†). The enhancement ratio for formate production with the Pd/C–Pt/C composite electrode is shown in Fig. 5d. The maximum value reaches 8.2 at -0.4 V as a result of the combination of thermocatalytic and electrocatalytic reduction of CO_2 .

Conclusions

In summary, a significant EPOC effect was observed over Pd NPs during CO_2 reduction to generate formate in 1 M KHCO_3 solution at ambient temperature. Both thermocatalytic and electrocatalytic reduction of CO_2 over Pd NPs were promoted by applying negative potentials and by adding H_2 to the feeds, respectively. The shared reaction intermediate HCOO^* over Pd NPs was proposed as the origin of the EPOC effect during the thermocatalytic and electrocatalytic reduction of CO_2 . Based on the abovementioned understanding, the Pd/C–Pt/C composite electrode was constructed for CO_2 reduction without the direct addition of H_2 to the feeds. H_2 generated through water electrolysis over Pt NPs effectively promoted the formate production over Pd NPs. The significant rate enhancement ratio for CO_2 reduction not only reveals a new example of EPOC in a low-temperature aqueous electrochemical reaction, but also provides an alternative strategy to promote the electrocatalytic reduction of CO_2 .

Acknowledgements

We gratefully acknowledge the financial support received from the Ministry of Science and Technology of China (Grants 2016YFB0600901 and 2013CB933100), the National Natural



Science Foundation of China (Grants 21573222 and 91545202), and the Strategic Priority Research Program of the Chinese Academy of Sciences (Grant No. XDB17020200). G. X. Wang would also like to thank the financial support received from CAS Youth Innovation Promotion.

References

- 1 M. Stoukides and C. G. Vayenas, *J. Catal.*, 1981, **70**, 137–146.
- 2 C. G. Vayenas, S. Bebelis and S. Ladas, *Nature*, 1990, **343**, 625–627.
- 3 C. G. Vayenas and C. G. Koutsodontis, *J. Chem. Phys.*, 2008, **128**, 182506.
- 4 C. G. Vayenas, *Catal. Lett.*, 2013, **143**, 1085–1097.
- 5 P. Vernoux, L. Lizarraga, M. N. Tsampas, F. M. Sapountzi, A. De Lucas-Consuegra, J. L. Valverde, S. Souentie, C. G. Vayenas, D. Tsiplakides, S. Balomenou and E. A. Baranova, *Chem. Rev.*, 2013, **113**, 8192–8260.
- 6 C. G. Vayenas and S. Brosda, *Top. Catal.*, 2014, **57**, 1287–1301.
- 7 D. Theleritis, S. Souentie, A. Siokou, A. Katsaounis and C. G. Vayenas, *ACS Catal.*, 2012, **2**, 770–780.
- 8 S. G. Neophytides, D. Tsiplakides, P. Sronehart, M. M. Jaksic and C. G. Vayenas, *Nature*, 1994, **370**, 45–47.
- 9 S. G. Neophytides, D. Tsiplakides, P. Stonehart, M. Jaksic and C. G. Vayenas, *J. Phys. Chem.*, 1996, **100**, 14803–14814.
- 10 M. Salazar and E. S. Smotkin, *J. Appl. Electrochem.*, 2006, **36**, 1237–1240.
- 11 L. Ploense, M. Salazar, B. Gurau and E. S. Smotkin, *J. Am. Chem. Soc.*, 1997, **119**, 11550–11551.
- 12 F. M. Sapountzi, M. N. Tsampas and C. G. Vayenas, *Catal. Today*, 2007, **127**, 295–303.
- 13 F. M. Sapountzi, M. N. Tsampas and C. G. Vayenas, *Catal. Today*, 2009, **146**, 319–325.
- 14 J. Sanabria-Chinchilla, K. Asazawa, T. Sakamoto, K. Yamada, H. Tanaka and P. Strasser, *J. Am. Chem. Soc.*, 2011, **133**, 5425–5431.
- 15 S. Gao, Y. Lin, X. C. Jiao, Y. F. Sun, Q. Q. Luo, W. H. Zhang, D. Q. Li, J. L. Yang and Y. Xie, *Nature*, 2016, **529**, 68–71.
- 16 X. Min and M. W. Kanan, *J. Am. Chem. Soc.*, 2015, **137**, 4701–4708.
- 17 R. Kortlever, I. Peters, S. Koper and M. T. M. Koper, *ACS Catal.*, 2015, **5**, 3916–3923.
- 18 Y. H. Chen and M. W. Kanan, *J. Am. Chem. Soc.*, 2012, **134**, 1986–1989.
- 19 S. Zhang, P. Kang and T. J. Meyer, *J. Am. Chem. Soc.*, 2014, **136**, 1734–1737.
- 20 W. C. Chueh, C. Falter, M. Abbott, D. Scipio, P. Furler, S. M. Haile and A. Steinfeld, *Science*, 2010, **330**, 1797–1801.
- 21 M. D. Porosoff, M. N. Myint, S. Kattel, Z. Xie, E. Gomez, P. Liu and J. G. Chen, *Angew. Chem., Int. Ed.*, 2015, **54**, 15501–15505.
- 22 Z. H. He, Q. L. Qian, J. Ma, Q. L. Meng, H. C. Zhou, J. L. Song, Z. M. Liu and B. X. Han, *Angew. Chem., Int. Ed.*, 2016, **55**, 737–741.
- 23 S. Kattel, W. Yu, X. Yang, B. Yan, Y. Huang, W. Wan, P. Liu and J. G. Chen, *Angew. Chem., Int. Ed.*, 2016, **55**, 7968–7973.
- 24 M. Liu, Y. Pang, B. Zhang, P. De Luna, O. Voznyy, J. Xu, X. Zheng, C. T. Dinh, F. Fan, C. Cao, F. P. de Arquer, T. S. Safaei, A. Mepham, A. Klinkova, E. Kumacheva, T. Filleter, D. Sinton, S. O. Kelley and E. H. Sargent, *Nature*, 2016, **537**, 382–386.
- 25 M. Asadi, K. Kim, C. Liu, A. V. Addepalli, P. Abbasi, P. Yasaei, P. Phillips, A. Behranginia, J. M. Cerrato, R. Haasch, P. Zapol, B. Kumar, R. F. Klie, J. Abiade, L. A. Curtiss and A. Salehi-Khojin, *Science*, 2016, **353**, 467–470.
- 26 S. Lin, C. S. Diercks, Y. B. Zhang, N. Kornienko, E. M. Nichols, Y. B. Zhao, A. R. Paris, D. Kim, P. Yang, O. M. Yaghi and C. J. Chang, *Science*, 2015, **349**, 1208–1213.
- 27 B. A. Rosen, A. Salehi-Khojin, M. R. Thorson, W. Zhu, D. T. Whipple, P. J. A. Kenis and R. I. Masel, *Science*, 2011, **334**, 643–644.
- 28 D. F. Gao, H. Zhou, J. Wang, S. Miao, F. Yang, G. X. Wang, J. Wang and X. H. Bao, *J. Am. Chem. Soc.*, 2015, **137**, 4288–4291.
- 29 M. W. Tew, J. T. Miller and J. A. van Bokhoven, *J. Phys. Chem. C*, 2009, **113**, 15140–15147.
- 30 D. L. Knies, V. Violante, K. S. Grabowski, J. Z. Hu, D. D. Dominguez, J. H. He, S. B. Qadri and G. K. Hubler, *J. Appl. Phys.*, 2012, **112**, 083510.
- 31 H. Yoshitake, T. Kikkawa and K.-I. Ota, *J. Electroanal. Chem.*, 1995, **390**, 91–97.
- 32 H. Yoshitake, G. Muto and K.-I. Ota, *J. Electroanal. Chem.*, 1996, **401**, 81–87.
- 33 Z. Serhan, C. Aroulanda and P. Lesot, *J. Phys. Chem. A*, 2016, **120**, 6076–6088.
- 34 G. Muto, H. Yoshitake, N. Kamiya and K.-I. Ota, *J. Electroanal. Chem.*, 1998, **457**, 99–107.
- 35 K. Jiang, K. Xu, S. Z. Zou and W. B. Cai, *J. Am. Chem. Soc.*, 2014, **136**, 4861–4864.
- 36 J. Y. Wang, H. X. Zhang, K. Jiang and W. B. Cai, *J. Am. Chem. Soc.*, 2011, **133**, 14876–14879.
- 37 H.-X. Zhang, S.-H. Wang, K. Jiang, T. André and W.-B. Cai, *J. Power Sources*, 2012, **199**, 165–169.
- 38 Z. A. Chase, J. L. Fulton, D. M. Camaioni, D. Mei, M. Balasubramanian, V.-T. Pham, C. Zhao, R. S. Weber, Y. Wang and J. A. Lercher, *J. Phys. Chem. C*, 2013, **117**, 17603–17612.
- 39 C. J. Stalder, S. Chao, D. P. Summers and M. S. Wrighton, *J. Am. Chem. Soc.*, 1983, **105**, 6318–6320.
- 40 C. Iwakura, S. Takezawa and H. Inoue, *J. Electroanal. Chem.*, 1998, **459**, 167–169.
- 41 H. Yoshitake, K. Takahashi and K.-I. Ota, *J. Chem. Soc., Faraday Trans.*, 1994, **90**, 155–159.
- 42 R. Kortlever, J. Shen, K. J. Schouten, F. Calle-Vallejo and M. T. Koper, *J. Phys. Chem. Lett.*, 2015, **6**, 4073–4082.
- 43 D. F. Gao, J. Wang, H. H. Wu, X. L. Jiang, S. Miao, G. X. Wang and X. H. Bao, *Electrochem. Commun.*, 2015, **55**, 1–5.
- 44 J. Durst, C. Simon, F. Hasche and H. A. Gasteiger, *J. Electrochem. Soc.*, 2014, **162**, F190–F203.

